Open access • Journal Article • DOI:10.1007/S12289-009-0664-9

Hypoelastic, hyperelastic, discrete and semi-discrete approaches for textile composite reinforcement forming — Source link

Philippe Boisse, Yamina Aimene, Yamina Aimene, Abdelwaheb Dogui ...+8 more authors

Institutions: University of Lyon, University of the French West Indies and Guiana, Eni

Published on: 01 Sep 2010 - International Journal of Material Forming (Springer-Verlag)

Topics: Hypoelastic material, Continuous modelling, Discrete element method, Hyperelastic material and Finite element method

Hypoelastic, hyperelastic, discrete and semi-discrete approaches for textile composite reinforcement forming

Philippe Boisse, Yamina Aimene, A. Dogui, Samia Dridi, Sébastien Gatouillat, Nahiene Hamila, M. A. Khan, Tarek Mabrouki, Fabrice Morestin, Emmanuelle Vidal-Salle

Hypoelastic, hyperelastic, discrete and semi-discrete approaches for textile composite reinforcement forming

Philippe Boisse · Yamina Aimène · Abdelwaheb Dogui · Samia Dridi · Sébastien Gatouillat · Nahiene Hamila · Muhammad Aurangzeb Khan · Tarek Mabrouki · Fabrice Morestin · Emmanuelle Vidal-Sallé

Abstract The clear multi-scale structure of composite textile reinforcements leads to develop continuous and discrete approaches for their forming simulations. In this paper two continuous modelling respectively based on a hypoelastic and hyperelastic constitutive model are presented. A discrete approach is also considered in which each yarn is modelled by shell finite elements and where the contact with friction and possible sliding between the yarns are taken into account. Finally the semi-discrete approach is presented in which the shell finite element interpolation involves continuity of the displacement field but where the internal virtual work is obtained as the sum of tension, in-plane shear and bending ones of all the woven unit cells within the element. The advantages and drawbacks of the different approaches are discussed.

Keywords Textile composites · Forming simulations · Continuous/discrete approaches · Hyperelasticity · Hypoelasticity · Semi-discrete finite element

P. Boisse (✉) · Y. Aimène · S. Dridi · S. Gatouillat · N. Hamila · M. Aurangzeb Khan · T. Mabrouki · F. Morestin · E. Vidal-Sallé
Université de Lyon, INSA-Lyon, LaMCoS,
Lyon 69621, France
e-mail: Philippe.Boisse@insa-lyon.fr

Y. Aimène
Université des Antilles et de la Guyane,
Cayenne 97300, France

A. Dogui · S. Dridi
Laboratory of Mechanical Engineering, ENI,
Monastir, Tunisia

Introduction

Forming composite reinforcements is a common process in composite manufacturing. In case of structural applications the reinforcements are usually made of continuous fibres. The achievement of a double curved shape can be obtained by the deformation of an initially flat fibrous reinforcement. This reinforcement can be dry (i.e. without resin) in the case of the preforming stage of LCM processes (Liquid Composite Moulding) [1, 2]. In these processes, the resin will be injected in a second stage on the so called preform. In the case of thermoset or thermoplastic prepregs the resin is present within the reinforcement during the forming stage but it is in a weak state (because it is not yet polymerized in case of thermoset prepregs, because the process is performed at high temperature in case of thermoplastic prepregs). In these last cases the resin is not hardened and the forming is mainly led by the reinforcement. The present paper mainly concerns the deformation of preforms for LCM processes. Nevertheless the deformation modes of a prepreg during draping are not fundamentally different. The material mechanical behaviour remains of same nature but some properties (such as in-plane shear stiffness) are increased.

The continuous reinforcements are textile materials made of continuous fibres. They can be 2D woven fabrics (plain, twill or satin weave), interlock fabrics where the different interlock layers are jointed by the weaving [3, 4], 3D fabrics [3, 5] or Non Crimp Fabrics (NCF) [6]. The standard fibres used in composite applications are made of carbon, glass or aramid. These fibres have a very small diameter (5 to 25 μm) in comparison to their length (the length of the part). Their assembly to the textile material leads to a very specific mechanical behaviour because some relative displacements between the fibres and the yarns are

possible. Consequently the particular mechanical behaviour is strongly led by the fibre directions. The stiffness in the fibre direction is high, especially in comparison to their density. The other rigidities of the reinforcement are due to transverse contact and friction between fibres and yarns. They are weak in comparison to the tensile stiffness. Nevertheless these mechanical properties (in plane shear, bending, transverse compression rigidities) are important to describe some aspects of the forming process, especially wrinkles. The in-plane shear behaviour prescribes the maximum shear angle i.e. the maximum change of angle between warp and weft yarns that is possible in the textile reinforcement without wrinkles.

The approaches to model the forming of textile composite reinforcements belong to two main families that are related to the scale at which the analysis is made. The textile reinforcement is a set of yarns (or fibres). The analysis of the deformation can be made considering and modelling each of these yarns (or fibres) and their interactions (contact with friction). In this case the approach is called discrete or mesoscopic. Of course the number of yarns is high and the interactions are complex. On the opposite, the continuous approaches consider a continuous medium juxtaposed with the fabric and the mechanical behaviour of which is equivalent to those of the textile reinforcement. This mechanical behaviour is complex because it concerns large strains and strong anisotropy. Furthermore, it strongly changes during the forming.

The present paper aims to present continuous and discrete approaches for thin (2D) composite reinforcements forming simulations. First, two continuous approaches are described within a membrane assumption. The first one is based on a hypoelastic model and the second on a hyperelastic one. Then simulations of woven fabric forming based on a discrete approach are presented. Finally a semi-discrete approach which is an intermediate method between continuous and discrete ones is presented. The advantages and drawbacks of the different approaches are discussed.

Specificities of the textile composite reinforcement mechanical behaviour

Internal structure

Textiles are made up of thousands of fibres combined in interlacing warp and weft tows (Figs. 1 and 2). This internal structure makes relative motion possible between fibres and between yarns, and this leads to very specific mechanical behaviour. The only high stiffness is the tensile stiffness in the fibre direction; all other rigidities (shear, bending, compaction) are much weaker. A woven fabric is intrinsically a multiscale material and, depending on the specific application of interest, one or more scales of the woven fabric have to be explored.

Three scales can be distinguished. The macroscopic scale refers to the whole component level, with dimensions in the order of some centimeters to several meters (Fig. 1a). At the mesoscopic scale, the woven reinforcement is seen as a set of yarns, respectively the warp and the weft (or fill) yarns in case of a woven fabric . Consequently, the corresponding working scale is the one of the yarn dimension, typically one to several millimetres. For periodic materials, mesoscopic models consider the smallest elementary pattern which can represent the whole fabric by several translations. That domain is called the Representative Unit Cell (RUC). Each yarn is made up of thousands of continuous fibres which interact (Fig. 2), and thus the interactions of the reinforcement can be analyzed at the microscopic scale. At the microscopic level, the characteristic dimension is about one to several micrometers. This is the only scale at which the material is actually continuous.

Continuous and discrete approaches

The deformation analysis of a textile composite reinforcement can be addressed at the three scales (macro-meso-micro) defined above.

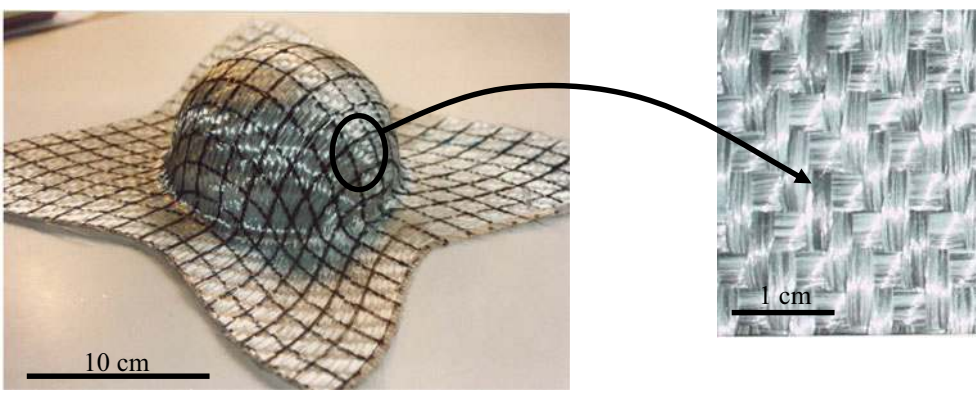

a Macroscopic scale **b** Mesoscopic scale

Fig. 1 Macroscopic and mesoscopic scales of textile composites reinforcements

Fig. 2 Yarn made of thousands of fibres

At macroscopic level, a woven fabric can be seen as a continuous material with a very specific mechanical behaviour, including high anisotropy and the ability to exhibit very large shearing and bending deformations. Investigation at the macroscopic level is the most popular for reinforcement forming simulations, as it allows using finite element codes with standard shell or membrane elements and does not ask the description of the internal textile material structure. Unfortunately, despite the large amount of work in this field [7–14] there is no widely accepted model that accurately describes all aspects of the mechanical behaviour of fabrics. Two continuous approaches are described in the present work in "Continuous approach 1: a hypoelastic model".

In discrete approaches, each yarn is modelled as a simple element such as a beam or spring and the interaction between warp and weft directions are taken into account explicitly by considering contact behaviour [6, 15–17]. Because this approach concerns the yarns it is also call meso-modelling. The main difficulty comes from the great number of yarns and of contacts that have to be taken into account. This is even more critical when the modelling is done at the microscopic level where each fibre is described as a beam [18–21]. For this reason, only very small fragment of the fabric can be modelled and this level is generally not suitable for forming simulations.

Continuous approach 1: a hypoelastic model

Hypoelastic models have been proposed for material at large strain [22, 23]:

$$\underline{\underline{\boldsymbol{\sigma}}}^{\nabla} = \underline{\underline{\mathbf{C}}} : \underline{\underline{\mathbf{D}}} \tag{1}$$

where $\underline{\underline{\mathbf{D}}}$ and $\underline{\underline{\underline{\underline{\mathbf{C}}}}}$ are the strain rate tensor and the constitutive tensor, respectively. $\underline{\underline{\sigma}}^{\nabla}$ called the objective derivative of the stress tensor, is the time derivative for an observer who is fixed with respect to the material.

$$\underline{\underline{\boldsymbol{\sigma}}}^{\nabla} = \underline{\underline{\mathbf{Q}}}.\left(\frac{\mathrm{d}}{\mathrm{dt}}\left(\underline{\underline{\mathbf{Q}}}^{\mathrm{T}}.\underline{\underline{\sigma}}.\underline{\underline{\mathbf{Q}}}\right)\right).\underline{\underline{\mathbf{Q}}}^{\mathrm{T}} \tag{2}$$

$\underline{\underline{\mathbf{Q}}}$ is the rotation from the initial orthogonal frame to the so-called rotating frame where the objective derivative is made. The most common objective derivatives are those of Green-Naghdi and Jaumann. They use the rotation of the polar decomposition of the deformation gradient tensor $\underline{\underline{\mathbf{F}}} = \underline{\underline{\mathbf{R}}}.\underline{\underline{\mathbf{U}}}$, (standard in Abaqus explicit), and the corotational frame, respectively. These are routinely used for analyses of metals at finite strains [24, 25].

It has been shown that, in the case of a material with one fibre direction the proper objective rotational derivative is based on the rotation of the fibre [26].

A membrane assumption is used. The Green-Naghdi's frame (GN) is the default work basis of ABAQUS/Explicit. Its unit vectors $\underline{\mathbf{e}}_1, \underline{\mathbf{e}}_2$ in the current configuration are updated from the initial orientation axes, $(\underline{\mathbf{e}}_1^0, \underline{\mathbf{e}}_2^0)$ using the proper rotation $\underline{\underline{\mathbf{R}}}$:

$$\underline{\mathbf{e}}_1 = \underline{\underline{\mathbf{R}}}.\underline{\mathbf{e}}_1^0 \quad \underline{\mathbf{e}}_2 = \underline{\underline{\mathbf{R}}}.\underline{\mathbf{e}}_2^0 \tag{3}$$

In the current configuration, the unit vectors in the warp and weft fibre directions are respectively:

$$\underline{\mathbf{f}}_1 = \frac{\underline{\underline{\mathbf{F}}}.\underline{\mathbf{f}}_1^0}{\left\|\underline{\underline{\mathbf{F}}}.\underline{\mathbf{f}}_1^0\right\|} \quad \underline{\mathbf{f}}_2 = \frac{\underline{\underline{\mathbf{F}}}.\underline{\mathbf{f}}_2^0}{\left\|\underline{\underline{\mathbf{F}}}.\underline{\mathbf{f}}_2^0\right\|} \tag{4}$$

Where $(\underline{\mathbf{e}}_1^0, \underline{\mathbf{e}}_2^0)$ and $(\underline{\mathbf{f}}_1^0, \underline{\mathbf{f}}_2^0)$ are assumed to coincide initially (Fig. 3). Two orthonormal frames based on the two fibre directions are defined: $\mathrm{g}\left(\underline{\mathbf{g}}_1, \underline{\mathbf{g}}_2\right)$ with $\underline{\mathbf{g}}_1 = \underline{\mathbf{f}}_1$ and $\mathrm{h}(\underline{\mathbf{h}}_1, \underline{\mathbf{h}}_2)$ with $\underline{\mathbf{h}}_2 = \underline{\mathbf{f}}_2$ (Fig. 3).

The strain increment $\underline{\underline{\mathbf{d}\boldsymbol{\varepsilon}}}$ is given as a code's output in calculation loop from time t^{n} to time $\mathrm{t}^{\mathrm{n+1}}$. (The matrix of the components of this strain increment is given in the GN frame in the case of ABAQUS/Explicit, but it could be any other frame). The components of the strain increment in the two frames g and h are considered (α and β are indexes taking value 1 or 2):

$$\underline{\underline{\mathbf{d}\boldsymbol{\varepsilon}}} = \mathrm{d}\varepsilon^{\mathrm{g}}_{\alpha\beta}\underline{\mathbf{g}}_{\alpha} \otimes \underline{\mathbf{g}}_{\beta} = \mathrm{d}\varepsilon^{\mathrm{h}}_{\alpha\beta}\underline{\mathbf{h}}_{\alpha} \otimes \underline{\mathbf{h}}_{\beta} \tag{5}$$

The fibre stretching strain and the shear strain are calculated for the two frames g and h.

$$\mathrm{d}\varepsilon^{\mathrm{g}}_{11} = \underline{\mathbf{g}}_1 \cdot \underline{\underline{\mathbf{d}\boldsymbol{\varepsilon}}} \cdot \underline{g}_1 \quad \mathrm{d}\varepsilon^{\mathrm{g}}_{12} = \underline{\mathbf{g}}_1 \cdot \underline{\underline{\mathbf{d}\boldsymbol{\varepsilon}}} \cdot \underline{\mathbf{g}}_2 \tag{6}$$

$$\mathrm{d}\varepsilon^{\mathrm{h}}_{22} = \underline{\mathbf{h}}_2 \cdot \underline{\underline{\mathbf{d}\boldsymbol{\varepsilon}}} \cdot \underline{\mathbf{h}}_2 \quad \mathrm{d}\varepsilon^{\mathrm{h}}_{12} = \underline{\mathbf{h}}_1 \cdot \underline{\underline{\mathbf{d}\boldsymbol{\varepsilon}}} \cdot \underline{\mathbf{h}}_2 \tag{7}$$

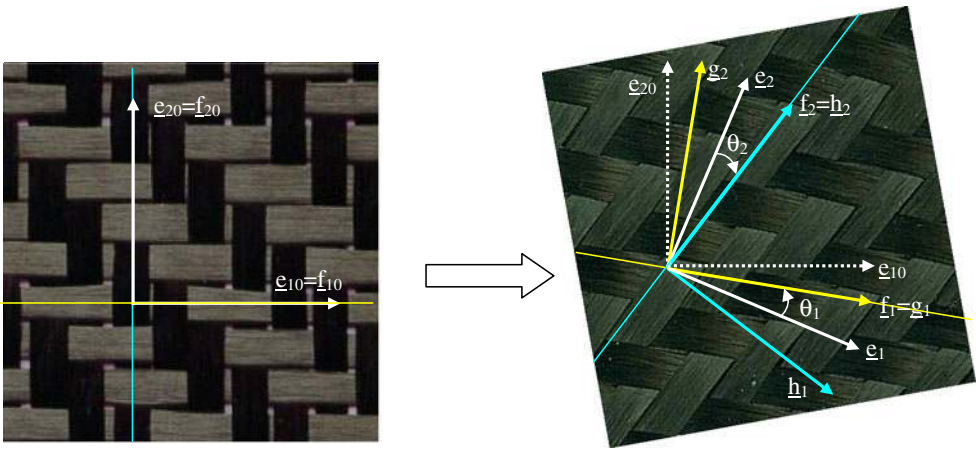

Fig. 3 Fibres axes and GN axes after deformation. Initially these axes are superimposed

From these strain components the axial stress component and shear stress components are calculated in each frame g and h:

$$d\sigma_{11}^{g} = E^{g} d\varepsilon_{11}^{g} \quad d\sigma_{12}^{g} = G d\varepsilon_{12}^{g} \tag{8}$$

$$d\sigma_{22}^{h} = E^{h} d\varepsilon_{22}^{h} \quad d\sigma_{12}^{h} = G d\varepsilon_{12}^{h} \tag{9}$$

E^g and E^h are the stiffness in the warp and weft fibre directions respectively and G the in-plane shear stiffness of the fabric (They are not constant, especially G depends strongly on the in plane shear). Following the scheme of Hughes and Winget [26, 27], the stresses are then integrated on the time increment from time t^n to time t^{n+1}:

$$\left(\sigma_{11}^{g}\right)^{n+1} = \left(\sigma_{11}^{g}\right)^{n} + d\sigma_{11}^{g^{n+1/2}} \quad \left(\sigma_{12}^{g}\right)^{n+1} = \left(\sigma_{12}^{g}\right)^{n} + d\sigma_{12}^{g^{n+1/2}} \tag{10}$$

$$\left(\sigma_{11}^{h}\right)^{n+1} = \left(\sigma_{11}^{h}\right)^{n} + d\sigma_{11}^{h^{n+1/2}} \quad \left(\sigma_{12}^{h}\right)^{n+1} = \left(\sigma_{12}^{h}\right)^{n} + d\sigma_{12}^{h^{n+1/2}} \tag{11}$$

The stress at time t^{n+1} in the fabric is the addition of the stresses in the two fibre frames:

$$\underline{\underline{\boldsymbol{\sigma}}}^{n+1} = \left(\underline{\underline{\boldsymbol{\sigma}}}^{g}\right)^{n+1} + \left(\underline{\underline{\boldsymbol{\sigma}}}^{h}\right)^{n+1} \tag{12}$$

For instance, denoting $\underline{\underline{\boldsymbol{\sigma}}} = \sigma_{\alpha\beta}^{e} \underline{\mathbf{e}}_{\alpha} \otimes \underline{\mathbf{e}}_{\beta}$ and omitting the superscript n+1 because all the quantities are at time t^{n+1}, the components of the Cauchy stress tensor in the GN frame (that are requested in the Abaqus Explicit code) are:

$$\sigma_{\alpha\beta}^{e} = \sigma_{11}^{g}\left(\underline{e}_{\alpha}.\underline{g}_{1}\right)\left(\underline{e}_{\beta}.\underline{g}_{1}\right) + \sigma_{22}^{h}(\underline{e}_{\alpha}.\underline{h}_{2})(\underline{e}_{\beta}.\underline{h}_{2}) + \sigma_{12}^{g}\left(\underline{e}_{\alpha}.\underline{g}_{1}\right)\left(\underline{e}_{\beta}.\underline{g}_{2}\right) + \sigma_{12}^{h}(\underline{e}_{\alpha}.\underline{h}_{1})(\underline{e}_{\beta}.\underline{h}_{2}) \tag{13}$$

Remark It is shown in Appendix A. that a shear angle increment $d\gamma$ gives stresses proportional to $Gd\gamma$. (γ is the shear angle, $\gamma = \theta_1 - \theta_2$ (Fig. 3)). That is important because the in-plane shear behaviour of a textile material is function of the shear angle (G is not constant and depends on γ).

More detail on this approach can be found in [28, 29]. This approach was used to simulate the forming of a double dome shape corresponding to an international benchmark [30]. An experimental device has been realised in INSA Lyon in order to perform this forming (Fig. 4). The woven

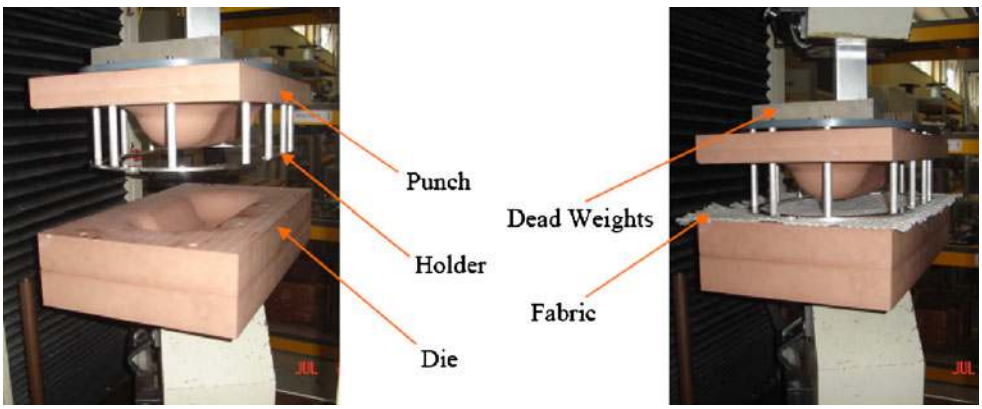

Fig. 4 Double dome forming: experimental device

fabric is a commingled glass/polypropylene plain weave that has been tested in the material benchmark study conducted recently [31]. The computed and experimental geometries after forming are compared Figs. 5 and 6. The shear angles have been measured using a 3D stereoscopic device [32]. The measured and numerical geometries and shear angles are in good agreement.

Continuous approach 2: a hyperelastic model

In this approach a potential is defined which aims to reproduce the non linear mechanical behaviour of textile composite reinforcements. The proposed potential is a function of the right Cauchy Green and structural tensor invariants defined from the fibre directions. This potential is based on the assumption that tensile and shear strain energies are uncoupled. It is the sum of three terms.

$$W = \overline{W}_1(I_1) + \overline{W}_2(I_2) + \overline{W}_S(I_{12}) \tag{14}$$

This assumption (tensile and shear strain energies are uncoupled) are made for sake of simplicity. The independence of tensile behaviour relatively to in plane shear has been shown experimentally [33]. The other hypotheses are probably less true, but there are very few data available on the couplings.

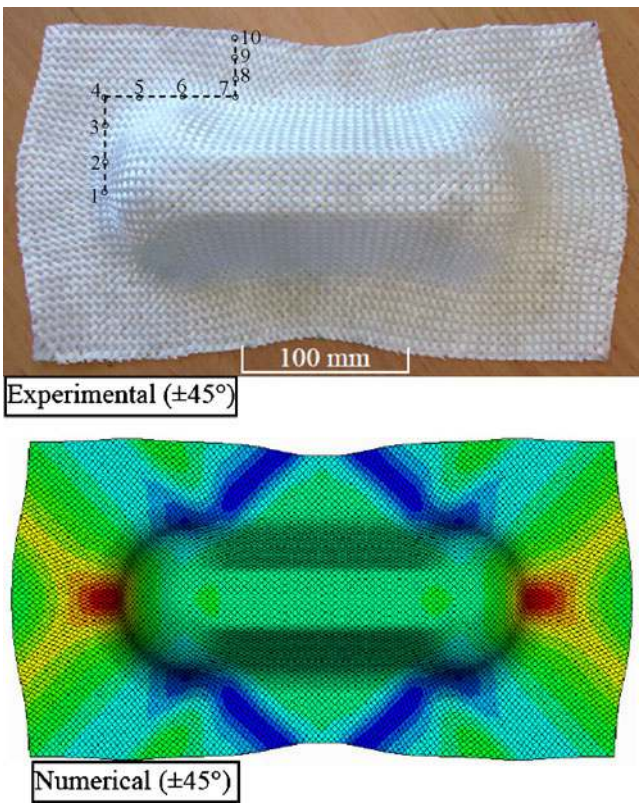

Fig. 5 Experimental and numerical outputs of double dome forming test

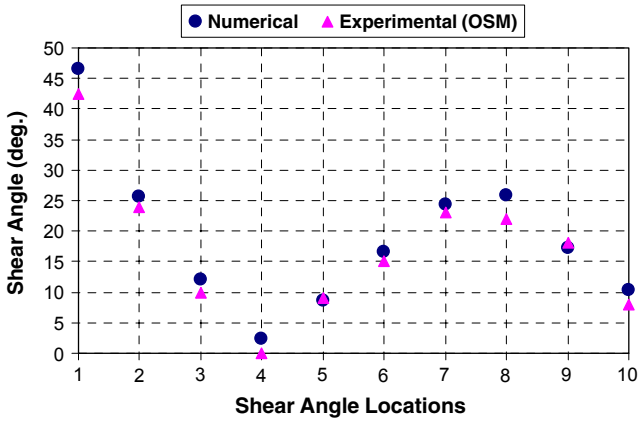

Fig. 6 Comparison between numerical and experimental shear angles at the locations shown in Fig. 5

The structural tensors $\underline{\underline{L}}_{\alpha\beta}$ are defined from the two unit vectors in the warp and weft directions $\underline{\mathbf{f}}_{10}$ and $\underline{\mathbf{f}}_{20}$ in the reference configuration C^0 (Fig. 3) [34]:

$$\underline{\underline{L}}_{\alpha\beta} = \underline{f}_{\alpha 0} \otimes \underline{f}_{\beta 0} \tag{15}$$

The two first terms $\overline{W}_1$ and $\overline{W}_2$ are the energies due to the tensions in the yarns. They are function of invariants I_1 and I_2 respectively, themselves depending on the right Cauchy Green strain tensor $\underline{\underline{C}} = \underline{\underline{F}}^T \cdot \underline{\underline{F}}$ and the structural tensors $\underline{\underline{L}}_{\alpha\alpha}$:

$$I_1 = \mathrm{Tr}\left(\underline{\underline{C}} \cdot \underline{\underline{L}}_{11}\right) = \lambda_1^2 \quad I_2 = \mathrm{Tr}\left(\underline{\underline{C}} \cdot \underline{\underline{L}}_{22}\right) = \lambda_2^2 \tag{16}$$

λ_α is the deformed length of on initially unit fibre in the direction α.

The third term $\overline{W}_S$ in (14) is a function of the second mixed invariants of $\underline{\underline{C}}$.

$$I_{12} = \frac{1}{I_1 I_2}\mathrm{Tr}\left(\underline{\underline{C}} \cdot \underline{\underline{L}}_{11} \cdot \underline{\underline{C}} \cdot \underline{\underline{L}}_{22}\right) = \cos^2\theta \tag{17}$$

The second Piola Kirchhoff stress tensor is derived from this potential [35–37]:

$$\underline{\underline{S}} = 2\frac{\partial W}{\partial \underline{\underline{C}}} \tag{18}$$

And in the case of the present potential (14):

$$\underline{\underline{S}} = 2\left[\frac{\partial \overline{W}}{\partial I_1} - \frac{I_{12}}{I_1}\frac{\partial \overline{W}}{\partial I_{12}}\right]\underline{\underline{L}}_{11} + 2\left[\frac{\partial \overline{W}}{\partial I_2} - \frac{I_{12}}{I_2}\frac{\partial \overline{W}}{\partial I_{12}}\right]\underline{\underline{L}}_{22} + 2\left[\sqrt{\frac{I_{12}}{I_1 I_2}}\frac{\partial \overline{W}}{\partial I_{12}}\right]\left(\underline{\underline{L}}_{12} + \underline{\underline{L}}_{21}\right) \tag{19}$$

In order to define the form of the potential two complementary assumptions are made taking into account the specific woven fabric behaviour and its deformation modes. As assumed above, i/ The tensions in the yarns and

the in-plane shear are independent. ii/ The tensions in the warp and weft directions are uncoupled.

The potential has to vanish in a stress free configuration. Polynomial functions of the invariants are considered in the present work. The global form of the proposed potential energy is given by:

$$W\left(\underline{\underline{C}}\right) = \sum_{i=0}^{r} \frac{1}{i+1} A_i \left(I_1^{i+1} - 1\right) + \sum_{j=0}^{s} \frac{1}{j+1} B_j \left(I_2^{j+1} - 1\right) + \sum_{k=1}^{t} \frac{1}{k} C_k I_{12}^k \qquad (20)$$

The resulting second Piola Kirchhoff tensor is:

$$\underline{\underline{S}} = 2 \left(\sum_{i=0}^{r} A_i I_1^i - \frac{1}{I_1} \sum_{k=1}^{t} C_k I_{12}^k \right) \underline{\underline{L}}_{11} + 2 \left(\sum_{j=0}^{s} B_j I_2^j - \frac{1}{I_2} \sum_{k=1}^{t} C_k I_{12}^k \right) \underline{\underline{L}}_{22} + 2 \left(\frac{1}{\sqrt{I_1 I_2}} \sum_{k=1}^{t} C_k I_{12}^{k-1/2} \right) \left(\underline{\underline{L}}_{12} + \underline{\underline{L}}_{21} \right) \qquad (21)$$

For strain-free configuration, stresses have to vanish. This condition imposes:

$$\sum_{i=0}^{r} A_i = 0 \quad ; \quad \sum_{j=0}^{s} B_j = 0 \qquad (22)$$

To determine the constants A_i, B_j and C_k, three experimental tests are necessary: two tensile tests in the warp and weft directions and one in-plane pure shear test. The details of the calculations to obtain Eqs. 19 to 21 are given in [38]. In this paper it is also shown that the form of the potential given above gives correct results concerning the direction of the loads on the boundary of a picture frame while other forms of the potential lead to boundary loads that are not correct for a woven fabric.

The proposed hyperelastic model is implemented in a user routine VUMAT of ABAQUS/Explicit and it is applied to membrane elements. The simulation of a hemispherical punch forming process is performed in the case of a strongly unbalanced twill [39]. The warp rigidity is 50 N/yarn and the weft rigidity is 0.2 N/yarn. The shear behaviour of this fabric has been experimentally analysed by the picture frame test [40]. The experimental results in terms of deformed shape are shown Fig. 7a together with the results of the simulation Fig. 7b. The computed deformed shape (made using the hyperelastic model proposed above) is in correct agreement with the experimental one. Especially the strong difference of the deformation in warp and weft directions is well verified. Another hyperelastic model applied to garment textile have been developed in [41].

A discrete approach for the composite reinforcement forming

In discrete modelling (also called meso-modelling in the case of textile material), the modelling does not directly concern the textile material but each fibre bundle. This one is modelled by elements simple enough to render the computation possible because it concerns the forming of the whole composite reinforcement and the number of yarns and contacts between these yarns is very large. The interactions between warp and weft directions are taken into account explicitly by considering contact behaviour and relative motions between the yarns are possible [15–17]. At the microscopic level, each fibre is satisfactorily described as a beam but this approach is time consuming.

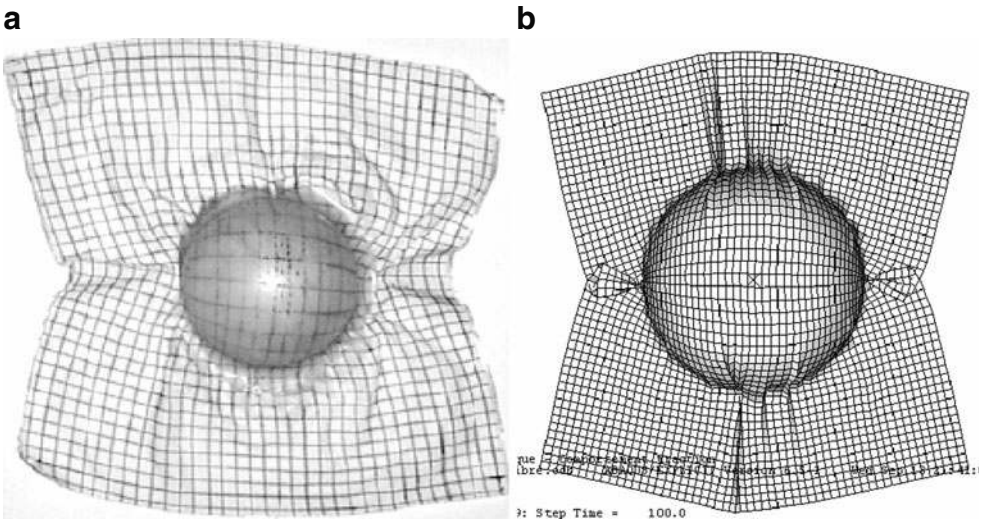

Fig. 7 Hemispherical forming of a very unbalanced woven fabric **a** experiment, **b** simulation using a hyperelastic model

The main difficulty is the great number of contacts with friction that have to be taken into account, especially for a woven fabric. For this reason, only very small elements of the fabric have been modelled to date [18, 20, 21]. Nevertheless, this approach is promising because it does not necessitate any assumptions regarding the continuity of the material, the specific mechanical properties resulting at the macroscopic level naturally follow the displacements and deformations of the yarns and it provides an interesting way of taking the weaving operation into account. The fibres constituting the yarns can be modelled directly, but their very large number (3K to 48K per yarn) requires that the computations are made for a number of fibres per yarn significantly smaller than in reality. An alternative possibility is to use a continuous behaviour for each yarn (meso-modelling). This implies that the fibrous nature of the yarn is taken into account in this model especially in order to have rigidities in bending and transverse compression very small in comparison to the tensile stiffness. In any case, a compromise must be found between a fine description (which will be expensive from the computation time point of view) and a model simple enough to compute the entire forming process. Figure 8b show the finite element model used for discrete simulations of forming processes (216 dof (degrees of freedom)). It is compared to another FE model of the unit cell used in [42] (Fig. 8a) to analyze the local in plane shear of a plain weave unit cell (47214 dof). It cannot be considered (at least today) to use this last FE model to simulate the forming of a composite reinforcement that is made of several thousands of woven cells. In the simplified unit cell (Fig. 8b) each yarn is described by few shell elements and the contact friction and possible relative displacement of the yarns are considered. The in-plane mechanical behaviour is the same as the one defined in [42] and is close of the one described in "Continuous approach 1: a hypoelastic model" (but for a single fibre direction). The bending stiffness is independent of the tensile one and very much reduced in comparison to the one given by plate theories.

Two examples are presented in Figs. 9 and 10 based on a discrete modelling using the unit cell of Fig. 8b. The first one is a picture frame test for which the wrinkles appear naturally in the simulation when the shear angle is reached. It must be noticed that the in-plane shear behaviour of the fabric is not an input data of the analysis and does not need to be known. It results at the macroscopic level of contact and friction between the yarns and lateral compression of the yarns. Figure 10 shows the results of a hemispherical forming simulation. It must be said that this study concerning forming simulation at the meso-scopic scale is beginning at INSA Lyon. If the discrete or mesoscopic modelling is a promising approach because a large part of the mechanical specificity of fabric behaviour is due to yarn and fibre interactions, and following fibre directions is simpler than for continuous models, it must be recognized that the forming simulations made with approaches that permits the relative sliding of the yarns in contact are not many. The simulation of impact in textile and textile composite may be more advanced but the physics of the deformation is somewhat different [43–45].

The semi-discrete finite elements for the composite reinforcement forming

This approach takes into account the difficulties to describe the textile material as a continuum in one hand (continuous approach) and the difficulties to model all the yarns and their contacts in the other hand (discrete approach). In this approach that is more or less intermediate, the textile composite reinforcement is seen as a set of a discrete number of unit woven cells submitted to membrane loadings (i.e. biaxial tension and in-plane shear) and bending (Fig. 11) [46, 47].

In any virtual displacement field $\underline{\eta}$ such as $\underline{\eta} = 0$ on the boundary with prescribed loads, the virtual work theorem relates the internal, exterior and acceleration virtual works:

$$W_{ext}(\underline{\eta}) - W_{int}(\underline{\eta}) = W_{acc}(\underline{\eta}) \tag{23}$$

with

$$W_{int}(\underline{\eta}) = W^{t}_{int}(\underline{\eta}) + W^{s}_{int}(\underline{\eta}) + W^{b}_{int}(\underline{\eta}) \tag{24}$$

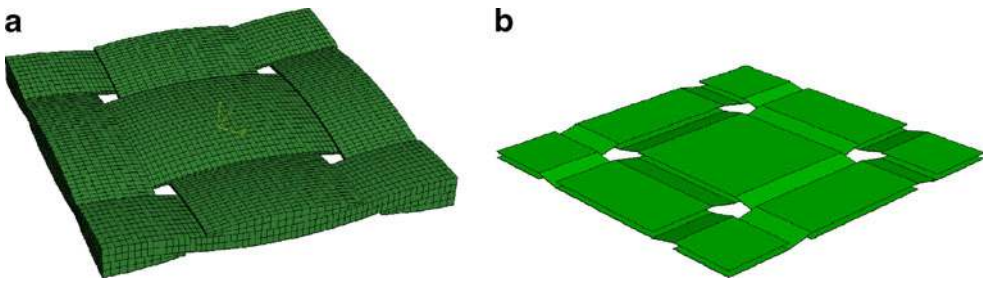

Fig. 8 Meso-modelling of a unit cell of a plain weave. (**a**) FE model for the analysis of the behavior of the unit cell. 47214 Dof. (**b**) FE model for simulations of the whole composite reinforcement forming. 216 Dof

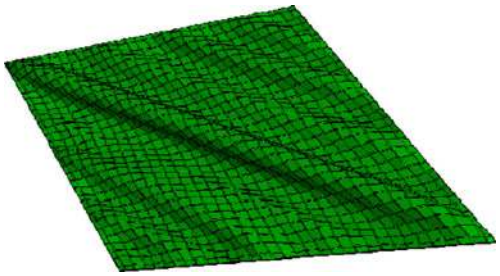

Fig. 9 Simulation of a picture frame test using the unit cell model of Fig. 8(b)

$W^{t}_{int}(\underline{\eta})$, $W^{s}_{int}(\underline{\eta})$, $W^{b}_{int}(\underline{\eta})$ are the internal virtual works of biaxial tension, in-plane shear and bending respectively with:

$$W^{t}_{int}(\underline{\eta}) = \sum_{p=1}^{ncell} {}^{p}\varepsilon_{11}(\underline{\eta})\,{}^{p}T^{11}\,{}^{p}L_1 + {}^{p}\varepsilon_{22}(\underline{\eta})\,{}^{p}T^{22}\,{}^{p}L_2 \quad (25)$$

$$W^{s}_{int}(\underline{\eta}) = \sum_{p=1}^{ncell} {}^{p}\gamma(\underline{\eta})\,{}^{p}M^{s} \quad (26)$$

$$W^{t}_{int}(\underline{\eta}) = \sum_{p=1}^{ncell} {}^{p}\chi_{11}(\underline{\eta})\,{}^{p}M^{11}\,{}^{p}L_1 + {}^{p}\chi_{22}(\underline{\eta})\,{}^{p}M^{22}\,{}^{p}L_2 \quad (27)$$

where ncell is the number of woven cell. L_1 and L_2 are the length of unit woven cell in warp and weft directions. $\varepsilon_{11}(\underline{\eta})$ and $\varepsilon_{22}(\underline{\eta})$ are the virtual axial strains in the warp and weft directions. $\gamma(\underline{\eta})$ is the virtual angle between warp and weft directions. $\chi_{11}(\underline{\eta})$ and $\chi_{22}(\underline{\eta})$ are the virtual curvatures of warp and weft yarns. $\varepsilon_{11}(\underline{\eta})$, $\varepsilon_{22}(\underline{\eta})$, $\gamma(\underline{\eta})$, $\chi_{11}(\underline{\eta})$ and $\chi_{22}(\underline{\eta})$ are function of the gradient of the virtual displacement field. T^{11} and T^{22} are the tensions on the unit woven cell in warp and weft directions. M^{11} and M^{22} are the bending moments on the woven cell respectively in warp and weft directions. M^{s} is the in-plane shear moment. The mechanical behaviour of the textile reinforcement defines a relation between the loads $T^{\alpha\alpha}$, M^{s}, $M^{\alpha\alpha}$ and the strain field. Experimental tests specific to textile composite reinforcements are used to obtain these mechanical properties. The biaxial tensile test gives the tensions T^{11} and T^{22} in function of the axial strain ε_{11} and ε_{22} [33], the picture frame or the bias extension test gives the shear moment M^{s} in function of the angle change γ between warp and weft yarns [31, 48] and the bending tests give the bending moments $M^{11}$and M^{22} in function respectively of χ_{11} and χ_{22} [49].

The tensions T^{11} and T^{22} simultaneously depend on the warp and weft strains because of the weaving i.e., they are in the form $T^{11}(\varepsilon_{11}, \varepsilon_{22})$, $T^{22}(\varepsilon_{11}, \varepsilon_{22})$. The in-plane shear moment is assumed to depend only on the shear angle i.e. M^{s} (γ). Bending moments are supposed to be in the form $M^{11}(\chi_{11})$ and $M^{22}(\chi_{22})$. The above forms of the loads $T^{\alpha\alpha}$, M^{s}, $M^{\alpha\alpha}$ in function of the strains in the unit woven cell are used because they account for the main phenomena, because other data are usually not available and also in order to keep the approach simple enough. Some studies have shown that these simplifications can be questionable in some cases [50, 51]. Nevertheless it is possible to extend the approach to the cases where each load $T^{\alpha\alpha}$, M^{s}, $M^{\alpha\alpha}$ depends on more strain components.

The three node triangle shown Fig. 11 is composed of ncelle woven cells. The virtual generalized strains $\varepsilon_{11}(\underline{\eta})$, $\varepsilon_{22}(\underline{\eta})$, $\gamma(\underline{\eta})$, $\chi_{11}(\underline{\eta})$ and $\chi_{22}(\underline{\eta})$ can be related to the virtual nodal displacements of the nodes of the element taking into account the interpolation of the geometric and kinematic conditions within the element. Especially, using a rotation free approach [52, 53], the curvatures $\chi_{11}(\underline{\eta})$, $\chi_{22}(\underline{\eta})$ are related to the virtual nodal displacement of the nodes 1, 2, 3 of the element and to those of the node 4, 5, 6 of the neighbouring triangles. This permits to define a shell element without rotation degrees of freedom. Using these strain interpolations in the internal virtual works defined Eqs. 23, 24 and 25 lead to the internal nodal loads of tensions, in-plane shear and bending respectively. Details of the expressions of these nodal loads can be found in [47].

The hemispherical forming of the very unbalanced twill (analysed in "Continuous approach 2: a hyperelastic model") is simulated using the semi-discrete elements defined above. The blank holder is a 6 kg ring submitted to its own weight. This final shape is well obtained by the simulation (Fig. 12). The ratio of the lengths after deformation lweft/lwarp is equal at the top of the hemisphere to 1.8 in experiments and in simulation as well. There are many wrinkles, especially along the vertical axis. They are fairly well obtained by the simulation.

Discussion and conclusion

Four different approaches have been presented in the paper. The two first ones ("Continuous approach 1: a hypoelastic

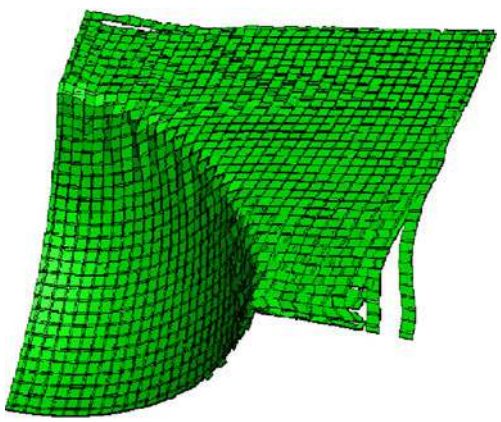

Fig. 10 Simulation of hemispherical forming test using the unit cell model of Fig. 8b

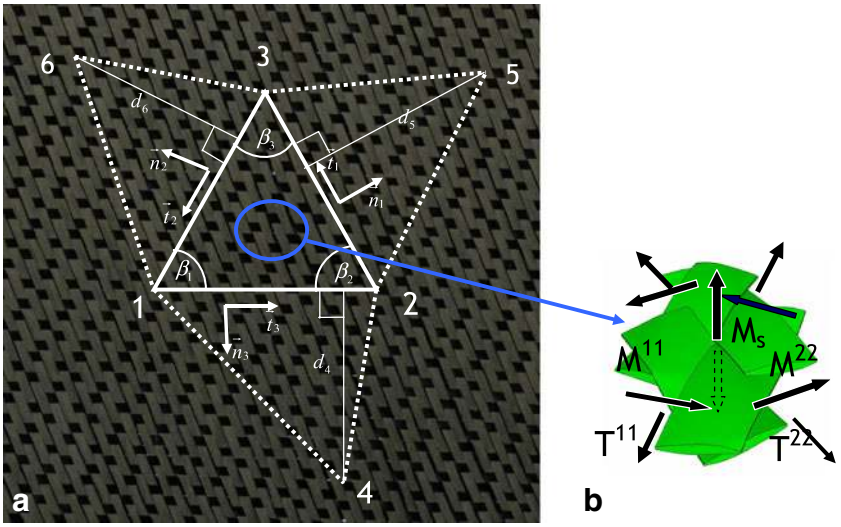

Fig. 11 Triangular finite element (**a**) made of unit woven cells submitted to tension, in-plane shear and bending (**b**)

model" and "Continuous approach 2: a hyperelastic model") are continuous approaches, the third one is a discrete modelling where each yarn is modelled as a set of shell elements ("A discrete approach for the composite reinforcement forming") and the fourth one is intermediate since the material is composed of a discrete number of unit woven cells but a continuity is due to the finite element interpolation (semi-discrete element, "The semi-discrete finite elements for the composite reinforcement forming").

The continuous approaches are made within membrane assumption while the two last one use shell finite elements. But this is not specific and all the presented approach can be made within membrane and shell assumption. The bending stiffness must be uncoupled with regard to the tensile rigidities. This stiffness is necessary to obtain correct shapes of the wrinkles. Nevertheless the membrane assumption is correct for most thin woven textile reinforcements. The appearance of wrinkles is due to compressive and above all to in-plane shear rigidities [46].

The discrete approach is attractive and promising. The very specific mechanical behaviour of the textile material due to the contacts and friction between the yarns and to the change of direction is implicitly taken into account. If some sliding occurs between warp and weft yarns, it can be simulated. This is not possible by the continuous approaches that consider the textile material as a continuum. This is an important point because it can be necessary to prevent such a sliding in a process. Nevertheless, the main drawback of the discrete approach is the necessary compromise that must be done between the accuracy of the

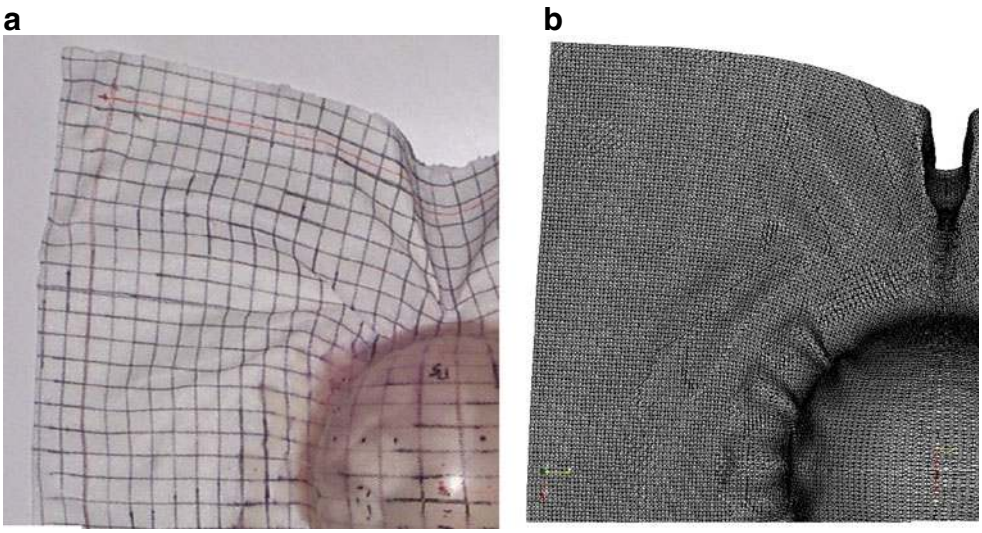

Fig. 12 Hemispherical forming of an unbalanced fabric. Experiment (**a**) and simulation using semi-discrete elements (**b**)

model of the unit woven cell and the total number of degrees of freedom. The modelling of the unit cell must be accurate enough to obtain a correct macroscopic mechanical behaviour, but the number of degrees of freedom of each cell must remain small in order to compute a forming process for which there will be thousands of woven cells. To our knowledge this discrete approach is not yet used in composite forming process simulations. There are a lot of improvements to achieve in the meso-modelling of different textile reinforcements. The continuous increase of the computer power is a strong argument in favour of this approach.

The continuous approach is the most commonly used in composite reinforcement forming today. The main advantage is to use standard shell or membrane finite element. The only mechanical behaviour has to be specified in order to take the very particular behaviour of textile materials into account. Many models exist, but none of them is clearly admitted. The modelling of a textile material at large strain is very difficult. We believe that one reason of this difficulty is due to the bad adequacy of the stress notion to the textile materials. A stress tensor associates an elementary surface load to a normal to an elementary surface. This is not clearly defined in the case of textile materials.

The semi-discrete approach aims to avoid the use of stress tensors and directly define the loading on a woven unit cell by the warp and weft tensions and by in-plane shear and bending moments. These quantities are simply defined on a woven unit cell and above all they are directly measured by standard tests on composite reinforcements (biaxial tension, picture frame, bias extension and bending tests). The virtual internal works within a fabric are obtained from these loads and moments and the dual virtual strains. This leads to simple and efficient elements. Among the different approach the best results have always been obtained in our lab by this semi-discrete approach, in particular on the tests that have been performed in comparison to experimental ones [54, 55]. An extension of the semi-discrete approach has been performed to the case of 3D interlock reinforcements used in aero engine fan blades [4].

Appendix A

γ is the shear angle, $\gamma = \theta_1 - \theta_2$ (Fig. 3). It is shown that a shear angle increment $d\gamma$ gives stresses proportional to $Gd\gamma$ in the stress computation scheme presented "Continuous approach 1: a hypoelastic model" (Eq. 3 to 11). That is important because the in-plane shear behaviour of a textile material is function of the shear angle (G is not a constant and depends on γ).

The polar rotation tensor and deformation gradient tensor are respectively:

$$\underline{\underline{\mathbf{R}}} = \underline{\mathbf{e}}_\alpha \otimes \underline{\mathbf{e}}_{\alpha 0} \quad \underline{\underline{\mathbf{F}}} = \lambda_\beta \underline{\mathbf{f}}_\beta \otimes \underline{\mathbf{e}}_{\beta 0} \tag{28}$$

λ_β is the deformed length of an initially unit fibre in the direction β. The right stretch tensor $\underline{\underline{\mathbf{U}}}$ is given by the polar decomposition:

$$\underline{\underline{\mathbf{U}}} = \underline{\underline{\mathbf{R}}}^{\mathrm{T}} \cdot \underline{\underline{\mathbf{F}}} = (\underline{\mathbf{e}}_{\alpha 0} \otimes \underline{\mathbf{e}}_\alpha) \cdot (\lambda_\beta \underline{\mathbf{f}}_\beta \otimes \underline{\mathbf{e}}_{\beta 0}) = (\lambda_\beta \underline{\mathbf{f}}_\beta \cdot \underline{\mathbf{e}}_\alpha)(\underline{\mathbf{e}}_{\alpha 0} \otimes \underline{\mathbf{e}}_{\beta 0}) \tag{29}$$

The symmetry of $\underline{\underline{\mathbf{U}}}$ imposes

$$\lambda_1 \underline{\mathbf{f}}_2 \cdot \underline{\mathbf{e}}_1 = \lambda_2 \underline{\mathbf{f}}_1 \cdot \underline{\mathbf{e}}_2 \tag{30}$$

In the case of pure in plane shear ($\lambda_1 = \lambda_2 = 1$) or in the case of equal fibre elongations in warp weft directions, this equation becomes

$$\underline{\mathbf{f}}_2 \cdot \underline{\mathbf{e}}_1 = \underline{\mathbf{f}}_1 \cdot \underline{\mathbf{e}}_2 \quad \text{or} \quad \underline{\mathbf{h}}_2 \cdot \underline{\mathbf{e}}_1 = \underline{\mathbf{g}}_1 \cdot \underline{\mathbf{e}}_2 \tag{31}$$

In the case of most of the composite reinforcements, the fibre elongations are small and (31) can be considered.

Because the frames $(\underline{\mathbf{e}}_1, \underline{\mathbf{e}}_2)$, $(\underline{\mathbf{g}}_1, \underline{\mathbf{g}}_2)$, $(\underline{\mathbf{h}}_1, \underline{\mathbf{h}}_2)$ are orthonormal

$$\underline{\mathbf{g}}_1 \cdot \underline{\mathbf{e}}_1 = \underline{\mathbf{g}}_2 \cdot \underline{\mathbf{e}}_2 \quad \underline{\mathbf{g}}_1 \cdot \underline{\mathbf{e}}_2 = -\underline{\mathbf{g}}_2 \cdot \underline{\mathbf{e}}_1 \tag{32}$$

$$\underline{\mathbf{h}}_1 \cdot \underline{\mathbf{e}}_1 = \underline{\mathbf{h}}_2 \cdot \underline{\mathbf{e}}_2 \quad \underline{\mathbf{h}}_1 \cdot \underline{\mathbf{e}}_2 = -\underline{\mathbf{h}}_2 \cdot \underline{\mathbf{e}}_1 \tag{33}$$

Considering a shear increment $d\gamma = d\theta_1 - d\theta_2 = d\varepsilon_{12}^{\mathrm{g}} - d\varepsilon_{12}^{\mathrm{h}}$, the Eqs. 31, 32, 33 lead to the specific form of the stress calculation Eq. 13:

$$\begin{aligned} d\sigma_{\alpha\beta}^{\mathrm{e}} &= G\left(d\varepsilon_{12}^{\mathrm{g}} - d\varepsilon_{12}^{\mathrm{h}}\right)\left(\underline{\mathbf{e}}_\alpha \cdot \underline{\mathbf{g}}_1\right)\left(\underline{\mathbf{e}}_\beta \cdot \underline{\mathbf{g}}_2\right) \\ &= G d\gamma \left(\underline{\mathbf{e}}_\alpha \cdot \underline{\mathbf{g}}_1\right)\left(\underline{\mathbf{e}}_\beta \cdot \underline{\mathbf{g}}_2\right) \end{aligned} \tag{34}$$

References

1. Advani SG (1994) Flow and rheology in polymeric composites manufacturing. Elsevier, Amsterdam
2. Saouab A, Bréard J, Lory P, Gardarein B, Bouquet G (2001) Injection simulations of thick composite parts manufactured by the RTM process. Compos Sci Technol 61:445–451
3. Mouritz AP, Bannister MK, Falzon PJ, Leong KH (1999) Review of applications for advanced three-dimensional fibre textile composites. Compos Part A 30:1445–1461
4. de Luycker E, Morestin F, Boisse P, Marsal D (2009) Simulation of 3D interlock composite preforming. Compos Struct 88:615–623
5. Tong L, Mouritz AP, Bannister MK (2002) 3D Fibre reinforced polymer composites. Elsevier Science, Oxford
6. Creech G, Pickett AK (2006) Meso-modelling of non-crimp fabric composites for coupled drape and failure analysis. J Mater Sci 41:6725–6736

7. Boisse P, Gasser A, Hagège B, Billoet JL (2005) Analysis of the mechanical behavior of woven fibrous material using virtual tests at the unit cell level. J Mater Sci 40:5955–5962
8. Dong L, Lekakou C, Bader MG (2001) Processing of composites: simulations of the draping of fabrics with updated material behaviour law. J Compos Mater 35:138–163
9. Hagège B, Boisse P, Billoët JL (2005) Finite element analyses of knitted composite reinforcement at large strain. European Journal of Computational Mechanics 14:767–776
10. Peng X, Cao J (2005) A continuum mechanics-based non-orthogonal constitutive model for woven composite fabrics. Compos Part A 36:859–874
11. Rogers TG (1989) Rheological characterisation of anisotropic materials. Composites 20:21–27
12. Spencer AJM (2000) Theory of fabric-reinforced viscous fluids. Compos Part A 31:1311–1321
13. ten Thije RHW, Akkerman R, Huétink J (2007) Large deformation simulation of anisotropic material using an updated Lagrangian finite element method. Comput Methods Appl Mech Eng 196:3141–3150
14. Yu WR, Pourboghrata F, Chungb K, Zampaloni M, Kang TJ (2002) Non-orthogonal constitutive equation for woven fabric reinforced thermoplastic composites. Compos Part A 33:1095–1105
15. Ben Boukaber B, Haussy G, Ganghoffer JF (2007) Discrete models of woven structures. Macroscopic approach. Compos Part B 38:498–505
16. Duhovic M, Bhattacharyya D (2006) Simulating the deformation mechanisms of knitted fabric composites. Compos Part A 37:1897–1915
17. Pickett AK, Creech G, de Luca P (2005) Simplified and advanced simulation methods for prediction of fabric draping. European Journal of Computational Mechanics 14:677–691
18. Zhou G, Sun X, Wang Y (2004) Multi-chain digital element analysis in textile mechanics. Compos Sci Technol 64:239–244
19. Durville D (2005) Numerical simulation of entangled materials mechanical properties. J Mater Sci 40:5941–5948
20. Durville D (2008) A finite element approach of the behaviour of woven materials at microscopic scale—11th Euromech-Mecamat conference—Mechanics of microstructured solids: cellular materials, fiber reinforced solids and soft tissues, Torino, Italia. arXiv: 0804.2952v1 [cond-mat.soft]
21. Miao Y, Zhou E, Wang Y, Cheeseman BA (2008) Mechanics of textile composites: micro-geometry. Compos Sci Technol 68:1671–1678
22. Truesdell C (1955) Hypo-elasticity. J Ration Mech Anal 4:83–133
23. Xiao H, Bruhns OT, Meyers A (1998) On objective corotational rates and their defining spin tensors. Int J Solids Struct 35:4001–4014
24. Belytschko T, Liu WK, Moran B (2000) Nonlinear finite elements for continua and structures. Wiley, Chichester
25. Crisfield MA (1997) Non-linear finite element analysis of solids and structures. Wiley, Chichester
26. Badel P, Gauthier S, Vidal-Sallé E, Boisse P (2008) Rate constitutive equations for computational analyses of textile composite reinforcement mechanical behaviour during forming. Compos Part A. doi:10.1016/j.compositesa.2008.04.015
27. Hughes TJR, Winget J (1980) Finite rotation effects in numerical integration of rate constitutive equations arising in large deformation analysis. Int J Numer Methods Eng 15:1862–1867
28. Khan MA, Mabrouki T, Boisse P (2009) Numerical and experimental forming analysis of woven Composites with double dome benchmark. Proceedings Esaform 2009, Springer
29. Khan MA (2009) Numerical and experimental analyses of woven composite reinforcement draping using a hypoelastic behaviour. Ph.D. Thesis, INSA Lyon
30. Woven composites benchmark forum. http://www.wovencomposites.org/. Accessed 11 May 2009
31. Cao J, Akkerman R, Boisse P, Chen J et al (2008) Characterization of mechanical behavior of woven fabrics: experimental methods and benchmark results. Compos Part A 39:1037–1053
32. Lomov SV, Boisse P, De Luycker E, Morestin F, Vanclooster K, Vandepitte D, Verpoest I, Willems A (2008) Full-field strain measurements in textile deformability studies. Compos Part A 39:1232–1244
33. Buet-Gautier K, Boisse P (2001) Experimental analysis and modeling of biaxial mechanical behavior of woven composite reinforcements. Exp Mech 41:260–269
34. Spencer AJM (1984) Continuum theory of the mechanics of fibres-reinforced composites. Springer-Verlag, New York
35. Basar Y, Weichert D (2000) Nonlinear continuum mechanics of solids. Springer, Berlin
36. Ogden RW (1984) Non-linear elastic deformations. Wiley, New York
37. Truesdell C, Noll W (1965) The nonlinear field theories of mechanics. Edition Handbuch der Physik Vol. III. Spinger, Berlin
38. Aimène Y, Vidal-Sallé E, Hagège B, Sidoroff F, Boisse P (2009) A hyperelastic approach for composite reinforcement large deformation analysis. J Compos Mater. doi:10.1177/0021998309345348
39. Daniel JL, Soulat D, Dumont F, Zouari B, Boisse P, Long AC (2003) Forming simulation of very unbalanced woven composite reinforcements. Int J Form Process 6:465–480
40. Dumont F (2003) Expérimentations et modèles de comportement de renforts de composites tissés. Ph.D. Thesis, Paris VI University
41. Dridi S (2009) Modélisation du comportement mécanique des textiles par des lois hyperélastiques. Ph.D. Thesis, University of Monastir and INSA Lyon, to appear
42. Badel P, Vidal-Sallé E, Maire E, Boisse P (2009) Simulation and tomography analysis of textile composite reinforcement deformation at the mesoscopic scale. Compos Sci Technol 68:2433–2440
43. Grave G, Birkefeld K, von Reden T, Drechsler K, Kyosev Y, Rathjens A (2009) Simulation of 3D overbraiding—solutions and challenges. Second World Conference on 3D Fabrics and their Applications, Greenville
44. Nilakantan G, Keefe M, Gillespie JW, Bogetti TA (2009) Simulating the impact of multi-layer fabric targets using a multi-scale model and the finite element method. Recent advances in textile composites. Proceedings of the 9th International Conference on Textile Composites—TEXCOMP9), DEStech Publications, Inc., 506–515
45. Sapozhnikov SB, Forental MV, Dolganina NY (2007) Improved methodology for ballistic limit and blunt trauma estimation for use with hybrid metal/textile body armor. Proceedings of the Conference Finite element modelling of textiles and textile composites (CD ROM), St-Petersburg
46. Boisse P, Zouari B, Daniel JL (2006) Importance of in-plane shear rigidity in finite element analyses of woven fabric composite preforming. Compos Part A 37:2201–2212
47. Hamila N, Boisse P, Sabourin F, Brunet M (2009) A semi-discrete shell finite element for textile composite reinforcement forming simulation. Int J Numer Methods Eng 79(12):1443–1466
48. Prodromou AG, Chen J (1997) On the relationship between shear angle and wrinkling of textile composite preforms. Compos Part A 28:491–503
49. de Bilbao E, Soulat D, Hivet G, Launay J, Gasser A (2008) Bending test of composite reinforcements. International Journal of Material Forming. doi:10.1007/s12289-008-0265-z
50. Launay J, Hivet G, Duong AV, Boisse P (2008) Experimental analysis of the influence of tensions on in plane shear behaviour of woven composite reinforcements. Compos Sci Technol 68:506–515

51. Lomov SV, Verpoest I (2006) Model of shear of woven fabric and parametric description of shear resistance of glass woven reinforcements. Compos Sci Technol 66:919–933
52. Sabourin F, Brunet M (1995) Analyses of plates and shells with a simplified 3 node triangular element. Thin-walled Struct 21:238–251
53. Onate E, Zarate F (2000) Rotation-free triangular plate and shell elements. Int Numer Methods Eng 47:557–603
54. Allaoui S, Boisse P, Chatel S, Hamila N, Hivet G, Soulat D (2009) Experimental and numerical analysis of a woven reinforcement forming process. Compos Part B, submitted
55. Hamila N, Boisse P, Chatel S (2008) Finite element simulation of composite reinforcement draping using a three node semi discrete triangle. International Journal of Material Forming 1:867–870. doi:10.1007/s12289-008-0-273-z